5-1-2015

Phase-Control of a Rising Sun Magnetron Using a Modulated, Addressable, Current Source

Sulmer Fernandez-Gutierrez
Bridge12

Jim Browning
Boise State University

Ming-Chieh Lin
Hanyang University

David N. Smithe
Tech-X Corporation

Jack Watrous
Confluent Sciences

Phase-control of a rising sun magnetron using a modulated, addressable, current source

Sulmer Fernandez-Gutierrez
Bridge12, 37 Loring Dr., Framingham, Massachusetts 01702

Jim Browning[a)]
Department of Electrical and Computer Engineering, Boise State University, 1910 University Dr., Boise, Idaho 83725

Ming-Chieh Lin
Department of Electrical and Biomedical Engineering, Hanyang University, Seoul 133-791, South Korea

David N. Smithe
Tech-X Corporation, 5621 Arapahoe Ave., Boulder, Colorado 80303

Jack Watrous
Confluent Sciences, LLC, Albuquerque, New Mexico 87111

(Received 5 December 2014; accepted 16 March 2015; published 1 April 2015)

It has been proposed that the use of gated field emitters with a faceted cathode in place of the conventional thermionic cathode could be used to control the current injection in a magnetron, both temporally and spatially. In this work, this concept is studied using the particle-in-cell code VORPAL. The magnetron studied is a ten-cavity, rising sun magnetron, which can be modeled easily using a 2D simulation. The magnetron has a ten-sided faceted cathode. The electrons are injected from three emitter elements on each of the ten facets. Each emitter is turned ON and OFF in sequence at the oscillating frequency with five emitter elements ON at once to obtain the five electron spokes of the π-mode. The simulation results show that the modulated, addressable cathode reduces startup time from 100 to 35 ns, increases the power density, controls the RF phase, and allows active phase control during oscillation. © *2015 American Vacuum Society*.
[http://dx.doi.org/10.1116/1.4916631]

I. INTRODUCTION

Microwave devices are capable of high output power (GW-class) with applications over a wide range of frequencies.[1–5] Magnetrons are used in numerous applications such as communication systems, radar, warfare, medical x-ray sources, and microwave ovens. Magnetrons are free running oscillators, so the phase is not controllable or stable during oscillation, and the magnetron start-up time may vary from pulse to pulse. It is desirable to phase control magnetrons to allow combining for high power applications and to allow applications such as phased array radar. Presently, power combining is performed by ganging magnetrons together using phase locking.[6–10] These magnetrons can be synchronized together and can be "phase locked" to a desired phase with the objective of getting a higher power output. We propose to control the phase of the magnetron by modulating discrete electron sources[11] at the magnetron operating frequency at the appropriate spatial locations to control the electron spoke formation. Typically, magnetrons use a thermionic cathode, but some magnetrons use ungated field emission cathodes[12,13] or secondary emission cathodes.[14,15] In these cases it is not practical to modulate the electron source at the device operating frequency. However, gated field emission arrays[16,17] could be used to provide a cathode which can be modulated at the magnetron operating frequency at discrete locations.

The use of gated vacuum field emitters[18,19] was proposed in a prior work[17] to replace conventional thermionic cathodes. This design offers a number of possible advantages: (1) the discrete current sources (emitters) provide a distributed cathode, (2) the electron source can be turned ON and OFF rapidly (<1 ns), and (3) the sources provide the means to spatially and temporally control the current injection. The spatial modulation improves the performance of the device by allowing the electron injection only at optimal locations where the greatest interaction occurs. The temporal modulation allows the control of the frequency and can be used to control the RF phase of the magnetron, and thus phase locking of multiple magnetrons.

This work involves the simulation of a 2D model of a ten-cavity rising sun magnetron device using the particle-in-cell (PIC) code VORPAL.[20] The simulation setup details and simulations using a continuous current source were presented in a prior work.[21] That work showed the simulations of a cylindrical, five-sided, and ten-sided cathode configuration. In this work, simulations of the temporal and spatial modulation of the current injection are studied implementing discrete (addressable) emitter sources on a ten-sided faceted cathode. With this technique, phase control is demonstrated at start-up, and phase locking is demonstrated by actively controlling the RF phase to generate a phase shift of 180°.

a)Electronic mail: jimbrowning@boisestate.edu

II. SIMULATION SETUP AND MODELING

The PIC code VORPAL is used to model a ten cavity rising sun magnetron with a ten-sided faceted cathode in 2D. The geometry and dimensions of the cathode are discussed here.[17,21] This geometry has an operating frequency of 957 MHz. One long cavity is loaded with an absorber to simulate the RF power dissipation in the device as well as the output power coupling. There is no other internal loss associated with the structure. This absorber is used to tune the quality factor, Q, of the magnetron which is 404 for the bulk of the work shown here.

The ten-sided cathode contains three emitter elements per facet, which can be turned ON and OFF at any desired time. Since this structure is a ten-cavity device, it has five spokes of electrons in the π-mode operation. Therefore, a single spoke rotates past two cathode facet plates (six emitter elements in total) every RF period. For this reason, five total emitter elements were turned ON simultaneously on every other facet at the same facet location at the frequency of operation (957 MHz) with an ON time of 1/6 $*\tau_{RF}$, where $\tau_{RF} = 1.04$ ns. Figure 1 shows the simulation for the ten-sided faceted cathode with modulated, addressable current sources but with the magnetic field turned off. This representation shows the emitters turning ON in sequence at different times for one total RF period. It can be seen that five emitter elements are initially turned ON at the same time on every other facet, and then these are followed by the remaining emitter elements as they complete the first RF period of the simulation.

The VORPAL simulation is set up with a grid of 202 × 202 to account for the needed spatial resolution of the finer facets and the emitter sections. The time step size was set to 1 ps, an integer fraction of the RF period; and the total run time was set to 150 ns. VORPAL implements the Dey–Mittra[22] cut-cell boundary algorithm to model curved boundaries, which is known to be a second order accurate.[23] This model was based on our previous work;[17,21] the operating parameters for this cathode geometry were set up as follows, a cathode–anode voltage (V_{ca}) of −22.2 kV, an applied magnetic field (B) of 0.09 T, and a total linear emitted current density (J'_e) of 326 A/m. Stability tests were also completed to study this model. The implementation in the simulation of a hybrid current source (continuous current emission and modulated current emission) was also performed to study the cause of gaps and holes observed in the electron spokes. This study will be discussed in more detail in Sec. III.

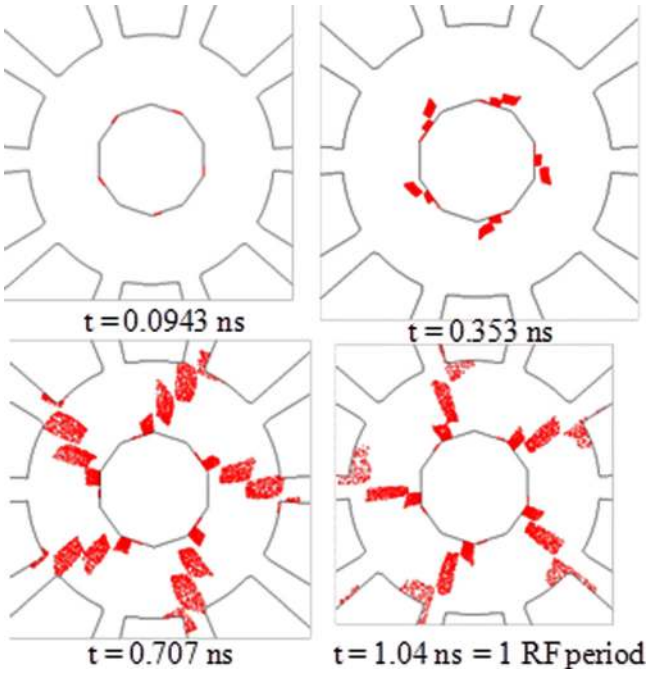

FIG. 1. (Color online) Ten-sided faceted cathode with modulated, addressable current sources, with B field turned OFF. This shows the emitters turning ON in sequence. The diagrams show one RF period (two facets), $\tau_{RF} = 1.04$ ns, $\Delta t = 1/6\ \tau_{RF}$. Frequency of modulation is 957 MHz.

III. RESULTS AND DISCUSSION

A. Modulated, addressable cathode

The simulations were run for the modulated current source as described above. Figure 2 shows the electron spokes at four different points in time during the magnetron start-up. Electron clumps are already visible at 40 ns; this time is much shorter than for a continuous current source[21] as will be discussed in detail later. These results demonstrate that the concept to modulate the current injection and control the spokes is viable. As one can see in the figure, the spokes initially tend to form electron clumps before they evolve into complete spokes. These electron clumps were seen as an initiation to the device spoke formation and oscillation. A similar behavior is observed in the transparent cathode magnetron developed by the University of New Mexico.[12] However, the two mechanisms of operation for the transparent cathode and the modulated, addressable cathode are

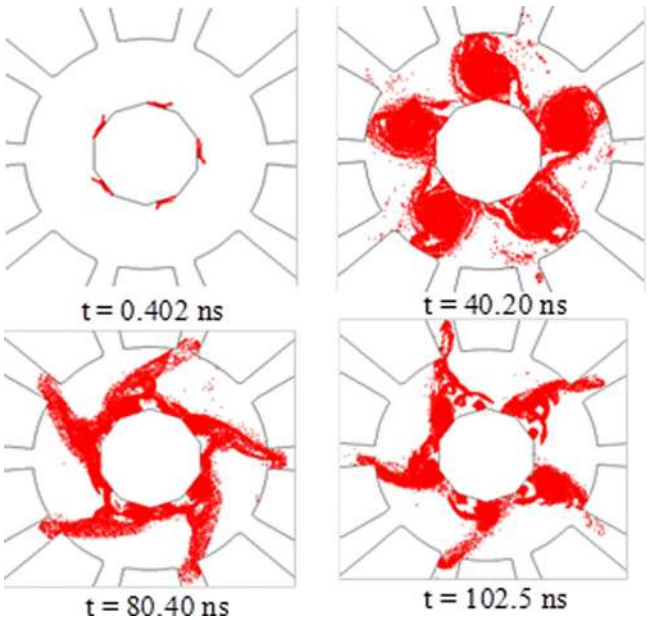

FIG. 2. (Color online) Ten-sided faceted cathode with modulated, addressable current sources. The frequency of modulation is 957 MHz, $\tau_{RF} = 1.04$ ns, $\Delta t = 1/6\ \tau_{RF}$.

different; nevertheless, the shape of the spokes as they start forming for both models is very similar. Gaps or voids are seen in the electron spokes; such gaps are not observed for normal continuous current operation.[21] These gaps appear to form because such a large fraction of the electrons are injected synchronously with the RF wave. Therefore, unusual trajectories, while still synchronous, are formed and voids in the spokes are created.

In order to check this hypothesis of void formation, a DC hub (continuous current emission) was implemented. The DC hub consists of a continuous current source that was turned ON together with the modulated current sources during the simulation. However, only a fraction of the total emitted current density is continuous while the rest is modulated. This approach provides a population of electrons that are not synchronous at injection and that can provide "fill current" for the spokes. These current fractions were varied, and the most stable case was used. The DC hub was turned ON at the start of the simulation, and the duration of the ON time was varied between 5 ns and total simulation run time. The total current of the DC hub was varied from 5% to 10% of the total emitted current. For the best case found, a 5% DC hub was used. Figure 3 shows the results using the DC hub. The green particles are the DC injected electrons, and the red particles are the modulated electrons. Note that in this figure, the green (continuous current) electrons are brought forward (cover the red electrons) to make them more visible since they represent only 5% of the injected electrons. It is observed that the DC hub successfully fills up the voids in the spokes as expected. Therefore, the DC hub could be used to minimize problems with the spoke formation in the modulated case.

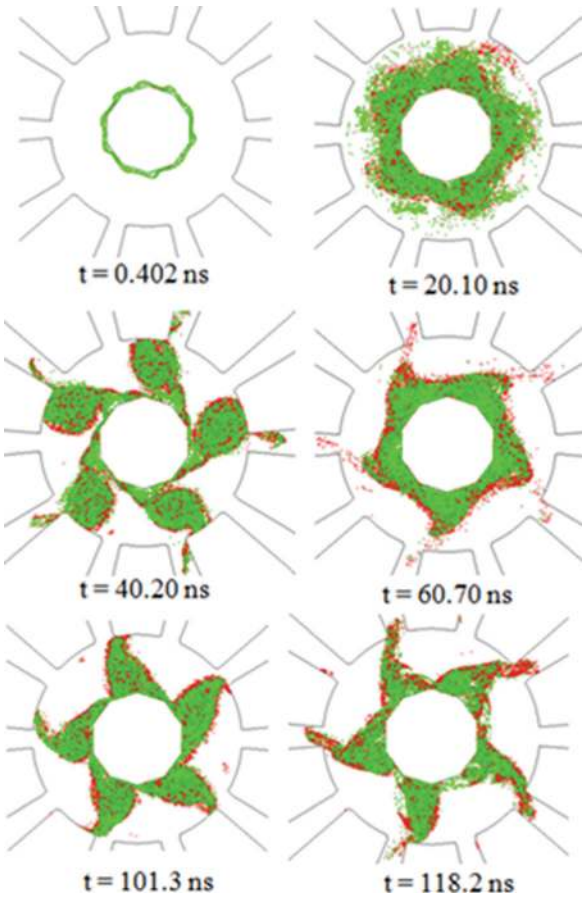

FIG. 3. (Color) Ten-sided faceted cathode with both a modulated, addressable current source (red particles) and a continuous current source (green particles). The green particles are brought forward and cover the red particles. This diagram shows a 5% continuous current (green electrons) fraction. The frequency of modulation is 957 MHz, $\tau_{RF} = 1.04$ ns, $\Delta t = 1/6\ \tau_{RF}$.

Figure 4(a) shows the cavity voltage frequency versus time for the modulated case. The startup time is indicated at ~50 ns based on the stability of the frequency as well as the spoke formation as explained in detail elsewhere.[11] Figure 4(b) shows the fast Fourier transform (FFT) of the time dependent cavity voltage measured in the simulations. As one can see in this plot, the frequency of operation for the device is at 957 MHz. It is also noted that a 650 MHz mode is present in this case. However, this lower frequency mode has a lower magnitude (approximately 20 dB) lower than the π mode and could be considered as noise. Furthermore, after ringing up the π mode, the resonance is stabilized, and this mode is no longer observed. For the lower frequency modes shown in the FFT plots, it only shows up in the transient period.

The startup time was also studied for the modulated case versus the typical continuous current source model.[21] Figure 5 shows the startup time versus injected current density for three cases: (1) a cylindrical cathode with continuous current, (2) a ten-sided cathode with continuous current, and (3) a ten-sided cathode with modulated current. The modulated case has a much shorter startup time with oscillations starting as soon as 35 ns. The modulation reduces startup time for all current densities as was expected given the synchronous, modulated electron injection. In general, the modulated case cuts the startup time by greater than 50%. As the current density is decreased, the startup time increases, but more slowly than for the continuous current cases. For currents

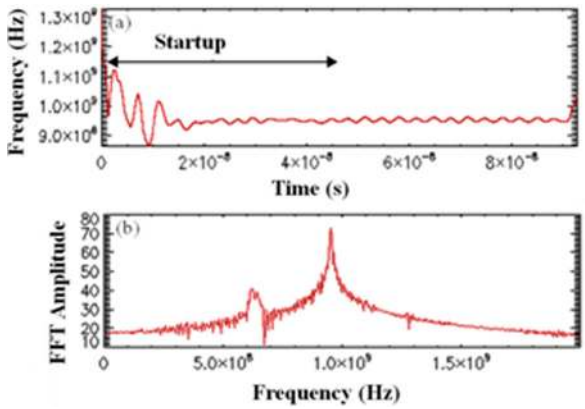

FIG. 4. (Color online) (a) Modulated ten-sided faceted cathode cavity voltage frequency vs time with moving window, showing the startup time of the device at 50 ns showing the operating frequency (π-mode) at 957 MHz from VORPAL; (b) FFT, over entire simulation time, of the loaded cavity voltage from VORPAL simulation. This plot indicates that the π-mode is dominant at the frequency of operation of 957 MHz. Reprinted with permission from Browning *et al.*, Appl. Phys. Lett. **104**, 233507 (2014). Copyright 2014, Applied Physics Letters.

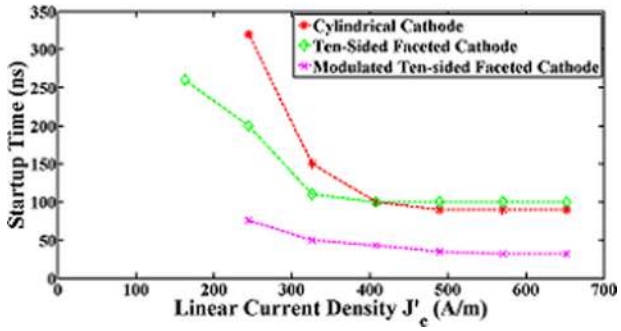

FIG. 5. (Color online) Comparison of startup time vs total emitted linear current density for different cathode geometries: cylindrical and faceted, including continuous current source model and the modulated, addressable current source model for the ten-sided faceted cathode.

<230 A/m, the modulated case switches completely to a lower mode (650 MHz frequency), and it never starts at the π-mode. The cause of this behavior needs further study.

B. Active phase control

The modulated, addressable cathode was studied to determine the phase of the oscillations. In prior work, separate simulations were run, and the locations of the electron spokes at specific moments in time[11] were compared. It was observed that the spokes are at the same exact location at the same simulation time for the modulated case. On the other hand, for the continuous current case,[21] the spokes are at three different locations at the same simulation time because of the random startup nature of the magnetron. This can also be studied by looking at the phase of the RF B_z-field versus number of RF periods after from a set reference time. The B_z-field was taken at the center of the loaded cavity. Figure 6 shows the RF phase difference versus RF periods for the modulated case and for the continuous current case during a simulation run. For the continuous current source model, it is observed that the phase difference is not constant, which is expected as a magnetron is a free running oscillator. However, for the modulated case the RF phase difference is constant; therefore, this result validates that the spokes are at the same location compared to a reference location and that the phase is controlled. From these results, it can be concluded that the modulated, addressable cathode controls the magnetron startup and RF phase.

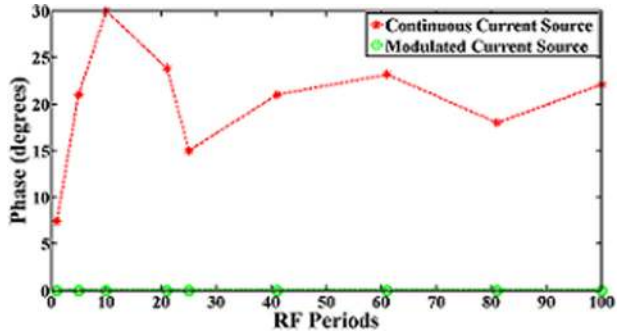

FIG. 6. (Color online) VORPAL simulation results showing the change in RF phase vs RF period from a reference point in a single simulation run for the continuous current source model and the modulated current source model.

Using the modulated, addressable cathode, the RF phase can also be dynamically controlled. For this simulation, the magnetron was allowed to reach stable oscillation. Then, at 88.40 ns, the electron injection was shifted in time (phase) to generate electron injection 180° out of phase with the ongoing oscillation. Figure 7 shows the RF B_z-field versus reference time (before phase shift) for this run. The RF B_z curves show the shift for 14, 17, and 35 RF periods after the reference point. Note that the x-axis is a referenced time for the purpose of showing the phase shift. The real time windows were chosen to cover these ranges: the phase 0° reference at t = 82 ns, phase difference = 88.5° at t = 96.8 ns, phase difference = 160.05° at 100 ns, and phase difference = 178.9° at t = 118.4 ns. These RF B_z curves also corroborate the results obtained by visually inspecting the spoke phase shift as described elsewhere.[11] Figure 8 shows a curve

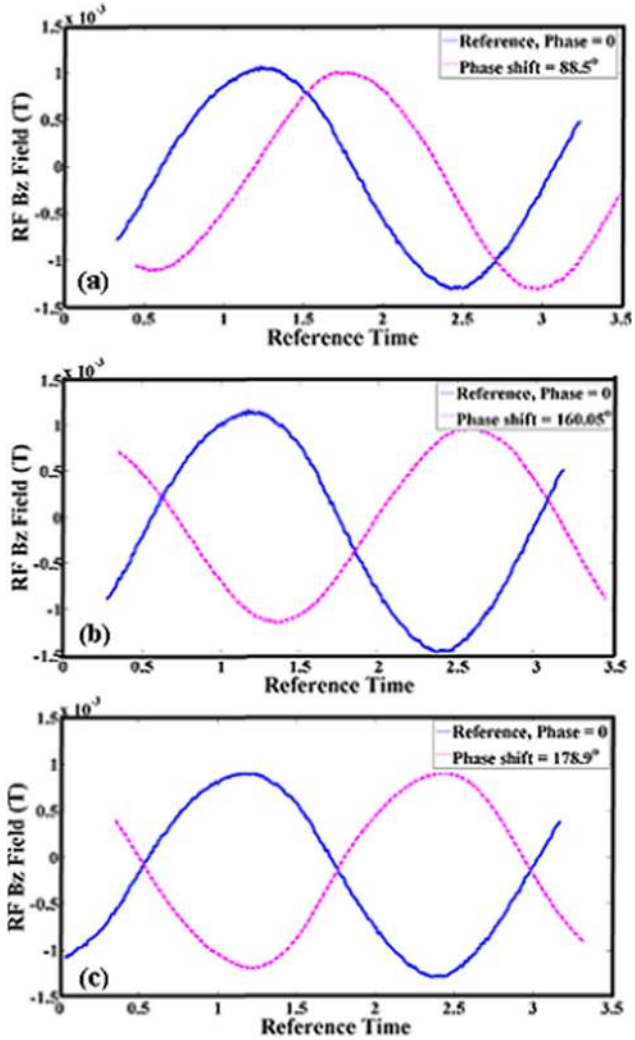

FIG. 7. (Color online) RF B_z field vs reference time; showing transition to a phase shift of 180° initiated at 88.40 ns. Reference: Phase = 0° (a) after 14.5 RF periods (t = 96.8 ns) from reference, 8 RF periods from phase shift, (b) after 17 RF periods (t = 100.0 ns) from reference, 11 RF periods from phase shift, and (c) after 35 RF periods (t = 118.4 ns) from reference, 29 RF periods from phase shift.

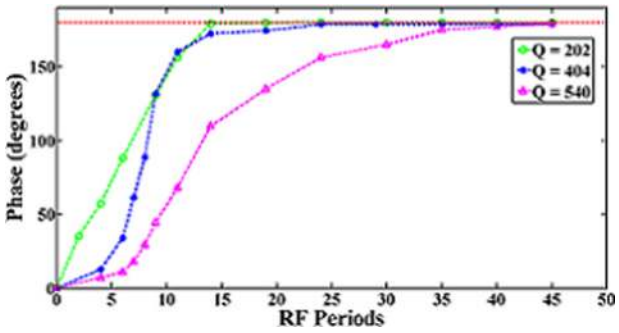

FIG. 8. (Color online) VORPAL simulation results showing the change in RF phase vs RF period for different values of Q after a 180° phase shift is generated using the modulated cathode. Phase was determined from the RF B_z component. Reprinted with permission from Browning *et al.*, Appl. Phys. Lett. **104**, 233507 (2014). Copyright 2014, Applied Physics Letters.

of the phase versus time. The phase is determined from the RF B_z plots referenced to the phase = 0° case. The graph shows the transition from 0° to 180°. The phase change occurs slowly until it completely transitions to steady state at 180°. This temporal transition is attributed to the quality factor, Q, of this magnetron. For high quality factors, typical of oscillators, it is difficult to have instant changes in phase, as was expected. It can be seen in the results that it takes approximately 25 RF periods after the phase change for the device to fully shift phase to 180° for the Q = 404 case, but for a case of Q = 540, the phase shift occurs in about 40 RF cycles, and for Q = 202, the phase shift occurs in about 14 RF cycles.

C. Power and efficiency

The power and efficiency were also studied for this model. The linear anode current density is used to determine the input power density for the magnetron. Figure 9 shows a plot of the anode current density, J'_a, versus the total emitted linear current density, J'_e, with the continuous current source and the modulated current source. The modulated cathode draws more current than the continuous cathode as expected. Because the electrons are injected in phase, they will be synchronous and will be more likely to give up energy and transit to the anode. Hence, there is an increase in the linear input power density for the modulated case. As can be

TABLE I. Cavity power and efficiency for different cathode geometries (CC, continuous current and MC, modulated current).

Cathode	Anode current density J'_a (A/m)	Pin (MW/m)	Loaded cavity power density (MW/m)	Efficiency η (%)
CC cylindrical	60.81	1.35	1.0	74.3
CC ten-sided	67.56	1.5	1.2	80.0
MC ten-sided	100	2.2	2.1	95.4

observed in the curves, the anode current density drawn by the device increases roughly linearly with the total emitted linear current density.

Table I shows a summary of results of the linear anode current density, the calculated input power density, the loaded cavity power, and the calculated efficiency for the modulated and continuous current source models at the reference parameters $V_{ca} = -22.2$ kV, $B = 0.09$ T, and $J'_e = 326$ A/m. It is observed that the loaded cavity power is very similar for the three cathode geometries with a continuous current source. The loaded cavity power results also show that the modulation technique increases the output power density and efficiency, as was expected, showing an efficiency of about 95.4%. For the modulated case, the anode current density increases to 100 A/m, and the output power approximately doubles to 2.1 MW/m. Overall, the efficiency increases from 80%–85% to 95%. Note, this efficiency should not be taken as absolute value and should only be used for comparison with the continuous current source cases. This is a 2D simulation, and there is no real output port; therefore, this power density is not the real coupled output power but the power generated with this loaded Q. In addition, the modulation power is ignored as discussed below. However, these results can be used as a relative estimation of the power at the loaded cavity as a demonstration of the modulated cathode increasing the loaded cavity power as was expected.

Figure 10 shows a graph of the loaded cavity power density versus the total emitted linear current density. It is observed that the loaded cavity power density curves present an almost linear increase in power as the emitted current

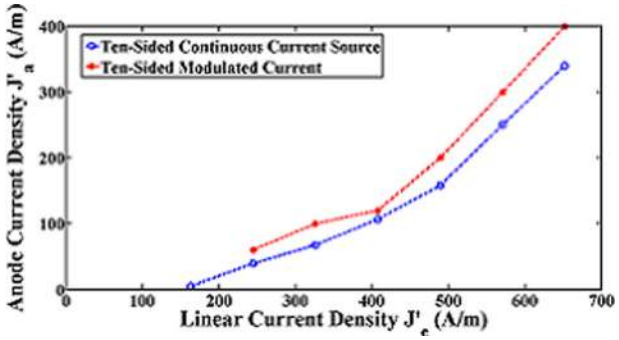

FIG. 9. (Color online) Anode current density vs total emitted linear current density for the ten-sided faceted cathode with continuous current source and modulated current source.

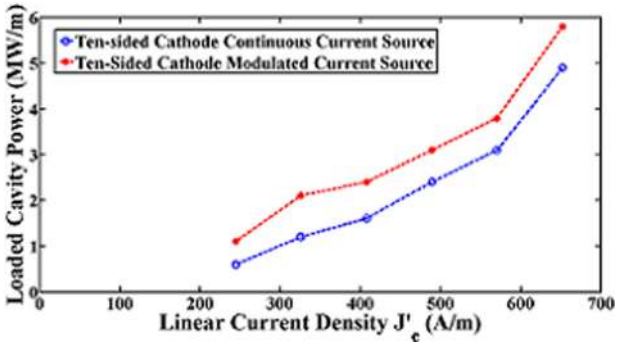

FIG. 10. (Color online) Loaded cavity power vs total emitted linear current density for the ten-sided faceted cathode with continuous current source and modulated current source.

density increases. This behavior is also comparable to the same linear increase in anode current as the total emitted current density increases in the previous figure. The power density goes up as the emitted current increases; it is clear from the curve that the modulated current model has a higher loaded cavity power density than the continuous current source model.

Figure 11 shows the plot of efficiency versus injected current density for both the continuous current source and the modulated current source model for the ten-sided faceted cathode. The modulated current curve shows higher efficiencies until $J'_e \approx 500$ A/m. It is observed that the maximum efficiency is obtained at the reference parameters $V_{ca} = -22.2$ kV, B = 0.09 T, and $J'_e = 326$ A/m in both models. As the current increases, the efficiency decreases, and the efficiency curves for the two cases (continuous and modulated current source) start to merge. At this point, for high current densities ($J'_e > 500$ A/m), the space charge effects become more significant, and the hub will get closer to the anode. This will result in the electrons having less potential energy to give up, and therefore, the loaded cavity power absorbed will be less. Even though the spokes are formed, they will start to spread out because of the space charge effects; therefore, the peak fields will saturate. This saturation will limit the device efficiency. Therefore, the advantages in power density and efficiency of using a modulated current source are no longer applicable for this regime.

This work presented the study of a modulated addressable cathode using discrete current sources modeled in VORPAL. Gated field emitters[16] are proposed for these modulated sources. They present a number of advantages, including a distributed cathode. These emitters can be turned ON and OFF with relatively low (<100 V) gate voltage; they can also be used in arrays, which allows spatial control of the current injection. In the case of the ten-sided faceted cathode the cathode-anode voltage is set to −22.2 kV with a total injected current of 32.6 A using an axial length of 10 cm.[17] Using the axial power density of 2.1 MW/m from the simulation, this device would generate an output power of about 210 kW. Each facet would emit 3.26 A. The current density of this device, if emitting from half of the cathode area, is ~1 A/cm^2, and it has been demonstrated that gated emitter arrays can work at current densities ~10 A/cm^2.[24,25] In addition, there is a cathode switching power associated with modulating the emitters, and this power can be calculated by using

$$P_s = \frac{1}{2} C_F V_F f, \tag{1}$$

where C_F is the emitter-gate capacitance, V_F is the emitter switching gate voltage, and f is the frequency of modulation. This power is not included in the efficiency calculations given above; although, for a practical application, using the results from this work and assuming a switching power of 10% of the power output (21 kW); the required capacitance can be estimated. For example, if emitting from half of the cathode area (~31 cm^2), with a typical emitter switching voltage of 100 V, the emitter capacitance must be <4.2 nF, which results in 134 pF/cm^2. This capacitance value is very small for gated field emitters; therefore, its application will require a much lower emitter voltage value (30–40 V) to allow for a higher capacitance [on the order of nF/cm^2 (Ref. 24)].

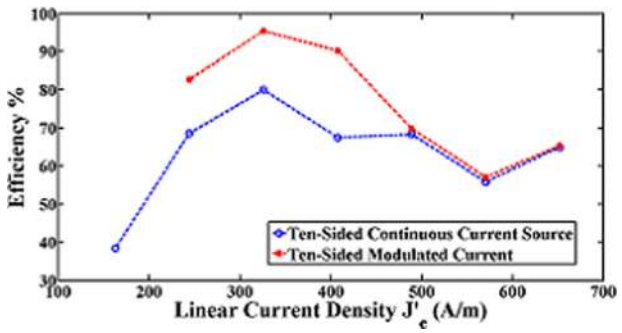

FIG. 11. (Color online) Efficiency vs total emitted linear current density for the ten-sided faceted cathode with continuous current source and modulated current source.

IV. CONCLUSIONS

The ten-sided faceted cathode with modulated current sources improved magnetron operation. It reduced the startup time from 110 to 50 ns for the reference case. It has been demonstrated that the shortest startup time can be as soon as 35 ns. The modulated cathode gave a higher cavity power density, about 80% increase resulting in higher efficiency. For the efficiency calculations, the axial losses (2D model) were not included. In addition, the modulated cathode requires power to turn the emitters ON and OFF. This switching power was not included in the efficiency calculation. It has also been demonstrated that the electron spoke locations and the RF phase can be controlled by the modulated cathode; therefore, such a magnetron would operate with true phase control and could easily be combined with other magnetrons for increased power or phased-array applications. Dynamic phase control is also demonstrated. Based on these results, the modulated, addressable cathode could be used for several applications and studies.

An electron source such as gated field emitters or photocathodes is proposed for the modulation. Such cathodes could be capable of producing the necessary current and temporal control that is needed for a practical device. Implementation of gated field emitters in such a configuration has been discussed elsewhere[17] where lateral gated emitters were proposed. The emitters would be placed below a slit structure to protect the emitters from the magnetron interaction space and ion back bombardment. The electrode at the exit of the slit structure fixes the electric field for the magnetron. Future work will include the study of a hybrid cathode approach where only a fraction of the injected current is modulated and will look at subharmonic modulation of the current to control phase. The simulation model will also be modified for 3D calculations. The 3D calculation would permit inclusion of a realistic Q-value through coupling to an extractor. The coupling to the extractor as well as

the effects of end-hats and external losses may all affect the device performance including the ability to control the phase.

ACKNOWLEDGMENTS

This research was supported by the Department of Electrical and Computer Engineering at Boise State University and the Air Force Office of Scientific Research. The authors also acknowledge the support provided by Tech-X Corporation in Boulder, CO.

[1]G. B. Collins, *Microwave Magnetrons.* (McGraw-Hill, New York, 1948).
[2]R. J. Barker, J. H. Booske, N. C. Luhmann, and G. S. Nusinovich, *Modern Microwave and Millimeter-Wave Power Electronics* (John Wiley & Sons, Inc., Piscataway, NJ, 2005).
[3]D. French, *Investigation of Novel Configurations for High Power Microwave Generation* (University of Michigan, Ann Arbor, MI, 2011).
[4]J. M. Osepchuk, IEEE Trans. Microwave Theory **50**, 975 (2002).
[5]S. Y. Liao, *Microwave Electron-Tube Devices* (Prentice-Hall, Englewood Cliffs, NJ, 1988).
[6]R. Adler, Proc. IRE **34**, 351 (1946).
[7]C. Dexter, G. Burt, R. G. Carter, I. Tahir, H. Wang, K. Davis, and R. Rimmer, Phys. Rev. Special Topics - Acc. Beams **14**, 032001 (2011).
[8]X. Chen, M. Esterson, and P. A. Lindsay, Proc. SPIE **2843**, 47 (1996).
[9]E. J. Cruz, *Peer-to Peer Magnetron Locking* (University of Michigan, Ann Arbor, MI, 2011).
[10]I. M. Rittersdorf, Y. Y. Lau, J. C. Zier, R. M. Gilgenbach, E. J. Cruz, and J. W. Luginsland, Appl. Phys. Lett. **97**, 171502 (2010).
[11]J. Browning, S. Fernandez-Gutierrez, M. C. Lin, D. N. Smithe, and J. Watrous, Appl. Phys. Lett. **104**, 233507 (2014).
[12]M. Fuks and E. Schamiloglu, Phys. Rev. Lett. **95**, 205101 (2005).
[13]D. A. Shiffler, M. Ruebush, M. LaCour, K. Golby, R. Umstattd, M. C. Clark, J. W. Luginsland, D. Zagar, and M. Sena, Appl. Phys. Lett. **79**, 2871 (2001).
[14]M. A. Kopot, V. D. Yeryomka, and V. P. Dzyuba, *IEEE International Conference on Vacuum Electronics (IVEC)* (2006), pp. 351–353.
[15]N. I. Avtomonov, D. M. Vavriv, and S. V. Sosnytsky, Radio. Comm. Syst. **53**, 1 (2010).
[16]S. G. Bandy, C. Spindt, M. A. Hollis, W. D. Palmer, B. Goplen, and E. G. Wintucky, *IEEE International Conference on Vacuum Microelectronics* (1998), pp. 132–133.
[17]J. Browning and J. Watrous, J. Vac. Sci. Technol. B **29**, 02B109 (2011).
[18]C. Spindt, C. Holland, and I. Schwoebel, *IEEE Electron Devices Meeting, IEDM '95* (1995), pp. 389–392.
[19]D. Temple, Mater. Sci. Eng., R **24**, 185 (1999).
[20]C. Nieter and J. R. Cary, J. Comput. Phys. **196**, 448 (2004).
[21]S. Fernandez-Gutierrez, J. Browning, M. C. Lin, D. N. Smithe, and J. Watrous, J. Vac. Sci. Technol. B **32**, 061205 (2014).
[22]S. Dey and R. Mittra, IEEE Microwave Guided Wave Lett. **7**, 273 (1997).
[23]C. Nieter, J. R. Cary, G. R. Werner, D. Smithe, and P. H. Stoltz, J. Comput. Phys. **228**, 7902 (2009).
[24]D. Whaley, B. Gannon, C. R. Smith, C. Armstrong, and C. Spindt, IEEE Trans. Plasma Sci. **28**, 727 (2000).
[25]A. Fomani, S. A. Guerrera, L. F. Velasquez-Garcia, and A. I. Akinwande, IEEE Trans. Electron Devices **61**, 2538 (2014).